Deposition of Nanostructured Thin Film from Size-Classified Nanoparticles

Renato P. Camata, Nicholas C. Cunningham
Department of Physics, University of Alabama at Birmingham, Birmingham, Alabama 35294-1170

Kwang Soo Seol, Yoshiki Okada, and Kazuo Takeuchi
Nanomaterials Processing Laboratory, The Institute of Physical and Chemical Research (RIKEN)
Wako, Saitama 351-0198, JAPAN.

Abstract

Materials comprising nanometer-sized grains (~1_50 nm) exhibit properties dramatically different from those of their homogeneous and uniform counterparts. These properties vary with size, shape, and composition of nanoscale grains. Thus, nanoparticles may be used as building blocks to engineer tailor-made artificial materials with desired properties, such as non-linear optical absorption, tunable light emission, charge-storage behavior, selective catalytic activity, and countless other characteristics. This bottom-up engineering approach requires exquisite control over nanoparticle size, shape, and composition. We describe the design and characterization of an aerosol system conceived for the deposition of size-classified nanoparticles whose performance is consistent with these strict demands. A nanoparticle aerosol is generated by laser ablation and sorted according to size using a differential mobility analyzer. Nanoparticles within a chosen window of sizes (e.g., (8.0±0.6) nm) are deposited electrostatically on a surface forming a film of the desired material. The system allows the assembly and engineering of thin films using size-classified nanoparticles as building blocks.

Introduction

An important thrust in current nanotechnology research is the idea of using nanoparticles as building blocks for the creation of advanced artificial materials [1]. One of the main reasons for this concept is the size-dependent properties exhibited by nanoparticles and nanocrystals. This opens the way for engineering the properties of a material by tuning the size of its individual constituents. However, the controlled assembly of materials systems from nanoparticles is a challenging endeavor and is being attempted by a variety of physical and chemical routes. Chemical strategies currently being explored involve molecular cross-linking [2], template patterning [3], solvent evaporation [4], and surfactant-assisted reverse micelle synthesis [5]. Given the complexity of the task, and the variety of physical systems of interest, alternative techniques are sought that can be generalized and combined with chemical routes to deliver these nanostructured materials with desired functionality.

Aerosol processes provide an interesting platform for controlled generation, assembly and deposition of nanostructured thin films from gas-borne nanoparticles. A promising aerosol strategy for the controlled synthesis of nanostructured materials involves continuous nanoparticle generation followed by size classification and subsequent deposition of size-selected nanoparticles on a solid substrate [6]. In this approach, an aerosol of nanoparticles of the material of interest (e.g., elemental, compound, organic) can be generated by a variety of methods such as spark discharge [6], thermal evaporation [7], and laser ablation [8]. Active aerosol size classification is then used to select only the desired nanoparticle size and subsequent deposition can lead to an extended ensemble of nanoparticles on a solid substrate. In this manner extended nanostructured films may be generated and their properties engineered to meet current needs for advanced materials.

This approach is endowed of remarkable flexibility as it can be applied to virtually any material that can be condensed from a vapor. Although this principle of material assembly has been demonstrated in a variety of contexts, the process has so far encountered serious limitations in applications that require significant nanoparticle throughput. There is great need to optimize the processes of generation, size classification, and deposition from the point of view of materials synthesis.

In this paper, we describe the design, characterization and performance of an aerosol instrument that tailors the processes of size classification and nanoparticle deposition for the specific purpose of fabrication of nanostructured thin films. As it will become clear in the following sections, two of the key issues addressed in this new instrument are the space charge and diffusion effects. Space-charge effects and diffusion losses are minimized by the careful choice of the design parameters and their optimization for operation in the 1-10 nm size range. The aerosol system developed is capable of performing size classification and deposition of a wide variety of nanoparticles and the design parameters have been optimized to enable high-resolution and high-throughput size classification and deposition of nanoparticles as small as 1 nm.

Size classification of aerosol nanoparticles

The differential mobility analyzer (DMA) is the key instrument in the measurement of ultrafine aerosol particles [9,10]. The DMA is the aerodynamic analog of a dispersive mass spectrometer. Physically, this instrument is a capacitor in which charged aerosol particles migrate across a laminar flow of a particle-free sheath gas as a result of an electric field. Because the particle electrical mobility is a function of its projected area, particles with different mobilities have distinct trajectories inside the DMA. A sampling orifice suitably placed at the analyzer electrode opposite to the aerosol inlet extracts only particles in a narrow window of mobilities. By varying the voltage across the capacitor, the applied field is varied and the mobility of the classified particles can be continuously tuned.

The basic physical principles that govern particle transport in this instrument are relatively simple and may be understood purely in terms of classical particle motion in a fluid suspension. Neglecting Brownian diffusion and space charge effects for the time being, the equation of motion of a particle suspended in a gas of viscosity μ and flowing with velocity $\vec{u}$ may be written from Newton's law simply as

$$m\frac{d\vec{v}}{dt} = \frac{3\pi\mu D_p}{C_c}\left(\vec{u} - \vec{v}\right) + q\vec{E} \tag{1}$$

where D_p, m, and q are the diameter, the mass, and the electric charge of the particle, respectively, and $\vec{E}$ is the applied electric field. The first term on the right-hand side of this equation is the drag force on a particle moving with velocity $\vec{v}$ in a fluid with velocity $\vec{u}$, and the second term is the electrical force. The quantity C_c is the slip correction factor which accounts for deviations from the Stokes drag for particles that are small compared to the mean free path of the gas molecules and is given by

$$C_c = 1 + Kn\left[\alpha + \beta\exp\left(-\frac{\gamma}{Kn}\right)\right] \tag{2}$$

where Kn is the Knudsen number, defined as the ratio of the gas mean free path to the particle radius (i.e., $Kn = 2\lambda/D_p$. The parameters α, β, and γ have been determined in numerous experiments [11]. The difference in the values of C_c for different sets of α, β, and γ is always below about 2% for Kn ranging from 0.001 to 100. Commonly accepted values are

$$\alpha = 1.257,\ \beta = 0.40,\ \gamma = 1.10 \tag{3}$$

and these will be used throughout this paper.

The steady state solution for Eq. (1) gives a particle migration velocity $\vec{v}$ parallel to the applied electric field $\vec{E}$.

$$\vec{v} = Z_p\vec{E} \tag{4}$$

where the proportionality constant, Z_p, is the particle electrical mobility which is defined as

$$Z_p = \frac{qC_c}{3\pi\mu D_p} \tag{5}$$

Thus, the electrical mobility of a particle and its migration velocity increase with decreasing particle size. This establishes the basis for size classification based on differences in particle mobility, provided that particles can be suitably extracted from the capacitor region without disturbing the flow and electric fields. As can be seen from Eq. (5), control over the charge state of the aerosol is also necessary for a one-to-one relationship between particle diameter D_p and electrical mobility Z_p. Multiply charged particles in the DMA will lead to multiple peaks in the size distribution of the classified aerosol.

Differential mobility analyzers are commonly implemented in a cylindrical geometry as illustrated in Fig. 1 In this configuration a sheath gas flows in the annulus between two concentric cylindrical electrodes with radii r_1 and r_2 at a volumetric rate Q_{sh} while the electrodes are maintained at a constant voltage difference. The aerosol is introduced in the annulus at a volumetric flow rate Q_a through a circular slit in the outer electrode and charged particles migrate toward the inner electrode due to the electrostatic force. Particles with electrical mobility within a certain range are extracted through a slit at the inner electrode by a sampling flow Q_s. If all charged particles have one elementary charge, the extracted particles are size classified and have a diameter $D_p \pm \Delta D_p$ [9].

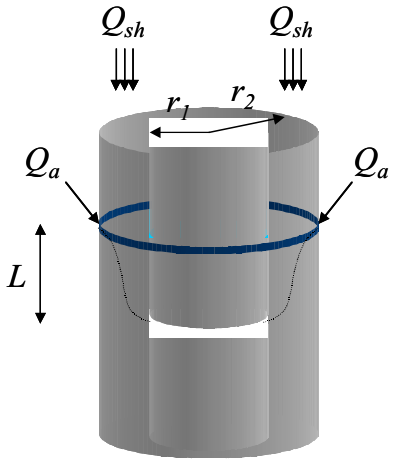

Fig. 1: Cylindrical geometry in which most differential mobility analyzers are implemented. The geometrical parameters are the radii of inner and outer electrodes (r_1 and r_2) and the length of the classification region (L).

Although this principle of size classification has now been applied in a variety of deposition experiments targeting the creation of new materials containing size-classified nanoparticles [6,12-16], the process has so far encountered serious limitations in applications that require significant nanoparticle throughput. This is because available DMAs have been developed to classify aerosols at relatively low concentrations ($<10^5$ cm^{-3}). Under these conditions, charged particle losses within the classification region of the DMA are small and space charge effects are expected to be minor. However, in applications of the DMA that involve high particle concentrations space charge effects cannot be ignored. Since DMAs are now being used to sort aerosol particles with respect to size to generate deposits for study of size dependent properties and fabrication of nanoparticle-based microelectronic and optical devices, the production of dense deposits in reasonable times, require that high concentration aerosols are processed through the DMA. When this is attempted, the performance of the size classification is seriously compromised due to the space charge field in the instrument [17].

We have devised a method to choose the values of the inner electrode radius r_1, the electrode separation r_2 - r_1, and the column length L of the DMA in order to maximize its throughput and resolution in a specific size range. Our method uses two factors to determine the best choice of r_1, r_2 - r_1, and L namely the space charge number Sc and the diffusion broadening parameter $\tilde{\sigma}$. A detailed explanation of the physical meaning of these quantities is provided in the sections that follow.

Minimizing space charge effects during size classification of nanoparticles

Materials synthesis from size-classified aerosol nanoparticles calls for the deposition of the gas-borne particles on a substrate. Assuming unity collection efficiency and neglecting particle pile-up, the time t required to generate a uniform one-monolayer deposit of singly charged nanoparticles over an area A is given by

$$t = \frac{4A}{NQ_s \pi D_p^2} \tag{6}$$

where D_p is the nanoparticle diameter, N is the particle number concentration and Q_s is the volumetric flow rate of the aerosol containing the classified particles. A plot of this equation as a function of number concentration is shown in Fig. 2 for the generation of a 1-mm diameter circular deposit using an aerosol flow rate of 1 SLM (standard liter per minute). This figure illustrates the need for high aerosol concentrations in the deposition of macroscopic amounts of size-classified nanoparticles. It is apparent that for low aerosol concentrations of 10^4 cm^{-3}, several days are necessary to deposit one monolayer of 10-nm particles. Deposits of smaller particles may demand weeks. Operation for such extended periods of time is usually impractical even for fully automated systems. High throughput and reasonable collection times can be achieved, however, if elevated number concentrations are processed in the DMA.

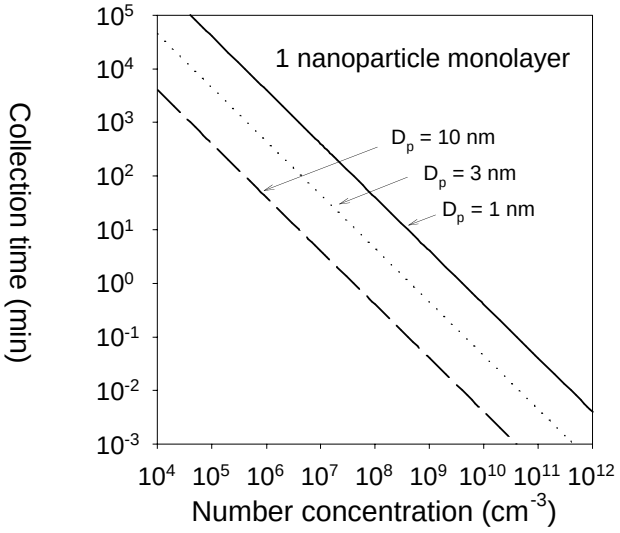

Fig. 2: Time required to deposit one nanoparticle monolayer as a function of number concentration for different particle diameters. Calculation for a nozzle-to-plane electrostatic precipitator with singly charged particles, aerosol flow rate of 1 SLM and deposit radius of 1 mm.

Ideally, one would like to perform size classification at concentrations in the 10^7 – 10^9 cm^{-3} range to generate deposits equivalent to several nanoparticle monolayers in a matter of hours or even minutes. Reliable operation in this regime would fully enable the size classification process as a materials processing technique.

Currently available DMAs cannot perform reliable size classification at these high number concentrations of charged particles. This is because under these conditions the electric field created by the particles undergoing classification becomes comparable to the applied electric field. Thus, space charge effects degrade the resolution and accuracy of the instrument.

However, changes of design parameters and operation conditions can help mitigate this problem. A useful guide in this area is the *space charge number*, Sc, a dimensionless group that roughly estimates the importance of the space charge field in a DMA [17]. Although this dimensionless group does not capture the details of the physical phenomenon involved, its scaling provides the essential features of the process and can be useful in the design of a DMA tailored for operation at high concentration of charged particles.

For a cylindrical DMA the space charge number may be written as [17]

$$\mathrm{Sc} = \frac{Ne}{\varepsilon V} G_F \tag{7}$$

where N is the concentration of charged particles in the DMA, e is the elementary charge, ε is the dielectric permittivity, V is the applied voltage, and G_F is a factor that depends on the flow rates and the geometry of the DMA [17]. This dimensionless group gives an idea of the importance of the space charge effect in a DMA under given operating conditions. Its value can be interpreted as an estimate, in percent, of the magnitude of the space charge field inside the DMA with respect to the applied electric field. Although helpful to elucidated the physical meaning of the space charge number, Eq. (7) is not in the appropriate form for our purposes. This is because in our analysis the voltage V also depends on r_1, r_2 - r_1, and L. Recollecting that

$$V = \frac{Q_{sh}}{2\pi L Z_p} \ln(r_2 / r_1) \tag{8}$$

and

$$Q_{sh} = \frac{\pi \nu \,\mathrm{Re}(r_2 + r_1)}{2(1+\beta)}, \tag{9}$$

where Re is the Reynolds number, ν is the fluid viscosity and β is given by

$$\beta \equiv \frac{Q_a + Q_s}{Q_e + Q_{sh}}, \tag{10}$$

the space charge number takes the form

$$\mathrm{Sc} = \frac{4Ne}{\varepsilon \nu \,\mathrm{Re}} \frac{(1+\beta)L}{(r_2 + r_1)\ln(r_2/r_1)} G_F(r_1, r_2, \beta) Z_p \tag{11}$$

The detailed expression for the factor G_F (r_1, r_2, β), which depends only on r_1, r_2, and β may be found in reference [17]. It is not included in Eq. (11) for the sake of simplicity.

A high-throughput DMA must be defined as an instrument that, for a given elevated concentration of charged particles N, presents Sc less than a few percent in order to avoid severe electric field distortions. Figure 3 presents a surface plot showing how the value of the space charge number Sc varies as a function of r_1 and r_2 - r_1. Not surprisingly, the figure shows that Sc is minimized when the electrode separation (i.e., r_2 - r_1) is minimized. This minimization of Sc leads to a maximized applied electric field and, consequently, to the minimization of space charge effects.

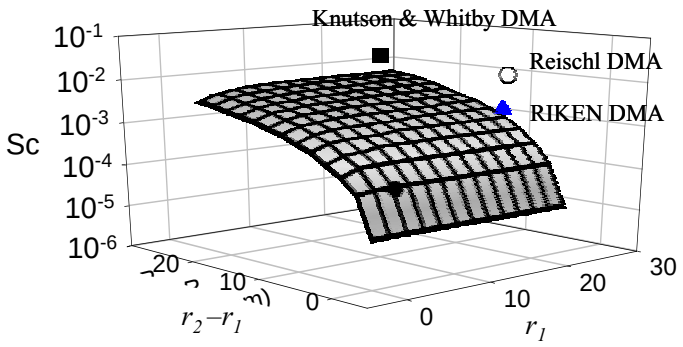

Fig. 3: Surface plot showing how the space charge number changes as a function of r_1 and r_2 - r_1 for $N = 10^9$ cm^{-3}, $\beta = 0.1$, $L = r_2 - r_1$, and $D_p = 1$ nm. The square (■), open circle (◦), and triangle (□) shown on the plot represent values of Sc for the same conditions for commercially available DMAs. The full circle (●) shows the value of Sc expected for the geometry we have chosen in our instrument.

Minimizing Brownian diffusion effects during size classification of nanoparticles

The physical mechanism that limits the resolution of aerosol size classification in a DMA is Brownian diffusion [18]. A simple model to predict the resolution of a DMA including Brownian diffusion effects was first introduced by Stolzenburg [19]. In a number of validation experiments this model has been found to describe the DMA performance satisfactorily in the nanometer size regime [19,20]. According to the model, the probability that a particle with a certain normalized mobility $\tilde{Z}_p \equiv Z_p / Z_p^*$ will be transmitted through the DMA is given by

$$\Omega(D_p) = \frac{\tilde{\sigma}}{\sqrt{2}\beta(1-\delta)}\left[\varepsilon\left(\frac{\tilde{Z}_p-(1+\beta)}{\sqrt{2}\tilde{\sigma}}\right)+\varepsilon\left(\frac{\tilde{Z}_p-(1-\beta)}{\sqrt{2}\tilde{\sigma}}\right)-\varepsilon\left(\frac{\tilde{Z}_p-(1+\beta\delta)}{\sqrt{2}\tilde{\sigma}}\right)-\varepsilon\left(\frac{\tilde{Z}_p-(1-\beta\delta)}{\sqrt{2}\tilde{\sigma}}\right)\right]$$

$$\beta \equiv \frac{Q_a + Q_s}{Q_e + Q_{sh}} \qquad (12)$$

$$\delta \equiv \frac{Q_a - Q_s}{Q_e + Q_{sh}}$$

where Q_a, Q_{sh}, Q_s, and Q_e are the aerosol, sheath, sample, and excess volumetric flow rates, respectively and $\varepsilon(x)$ is defined in terms of the error function erf(x) as

$$\varepsilon(x) \equiv \int_0^x erf(u)du = xerf(x) + \frac{1}{\sqrt{\pi}}\exp(-x^2) \qquad (13)$$

An inspection of Eqs. (12) reveals that the broadening parameter $\tilde{\sigma}$ is the quantity that determines the DMA resolution. For a cylindrical DMA and assuming plug flow, $\tilde{\sigma}$ may be found from [21]

$$\tilde{\sigma} = \frac{8D(D_p)}{\upsilon \mathrm{Re}}\left(\frac{1+\beta}{r_2-r_1}\right)\left[\frac{r_2^2+r_1^2}{r_2^2-r_1^2}(1+\beta)^2 L + \frac{r_2^2-r_1^2}{2}\frac{1}{L}\right] \qquad (14)$$

where $D(D_p)$ is the nanoparticle diffusivity, ν is the gas kinetic viscosity, and Re is the Reynolds number.

A large value of $\tilde{\sigma}$ corresponds to low resolution. Thus, the best DMA resolution is attained when $\tilde{\sigma}$ is minimized. According to Eq. (14), for a given particle size and flow rate regime, a choice of r_1 and $r_2 - r_1$ leads to a value of $L=L_{min}$ that minimizes $\tilde{\sigma}$. Figure 4 shows a surface plot of how $\tilde{\sigma}$ changes as a function of r_1 and $r_2 - r_1$. For every point on the surface, $L=L_{min}$ for particles with D_p = 1 nm. Due to the inherent nature of aerodynamic processes, there exists a limit in the practically achievable size resolution of an aerodynamic spectrometer like the DMA. This limit is believed to lie in the 3-5% range [22]. Thus, an instrument that can perform classification at a size resolution better than 5% is considered a high-resolution device.

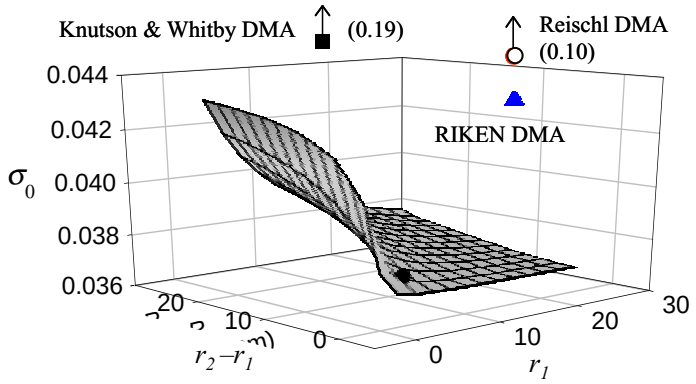

Fig. 4: Surface plot showing how the broadening parameter $\tilde{\sigma}$ changes as a function of r_1 and r_2 - r_1 for $L=L_{min}$, D_p = 1 nm, Re = 2200, β = 0.01, $L = r_2$ - r_1 (assuming plug flow). The square (■), open circle (¶), and triangle (□) shown on the plot represent values of $\tilde{\sigma}$ for the same conditions for commercially available DMAs. The full circle (●) shows the value of Sc expected for the geometry we have chosen in our instrument.

An instrument that simultaneously minimizes space charge and diffusion broadening

In this work we have designed an instrument for high-resolution size classification of particles in the 1-nm range that also meets the requirement for high throughput. This instrument achieves this high performance because its values of r_1, $r_2 - r_1$, and L have been chosen in order to minimize $\tilde{\sigma}$ and the space charge number Sc simultaneously. According to Eqs. (11) and (14) maximum throughput is enabled when Sc is minimized while maximum resolution is achieved when $\tilde{\sigma}$ is minimized. In order to perform size classification at high-throughput (up to 10^9 particles/cm^3 with less than 5% electric field distortion) and high-resolution (less than 5% size dispersion) the following conditions must be satisfied simultaneously

$$Sc < 0.05 \tag{15}$$

$$\tilde{\sigma} < 0.05 \tag{16}$$

Figure 5 shows the region in the $r_2 - r_1$ vs. r_1 space where the conditions of Eqs. (15) and (16) are satisfied simultaneously. The figure also shows the region of acceptable flow rates (less than 50 SLM).

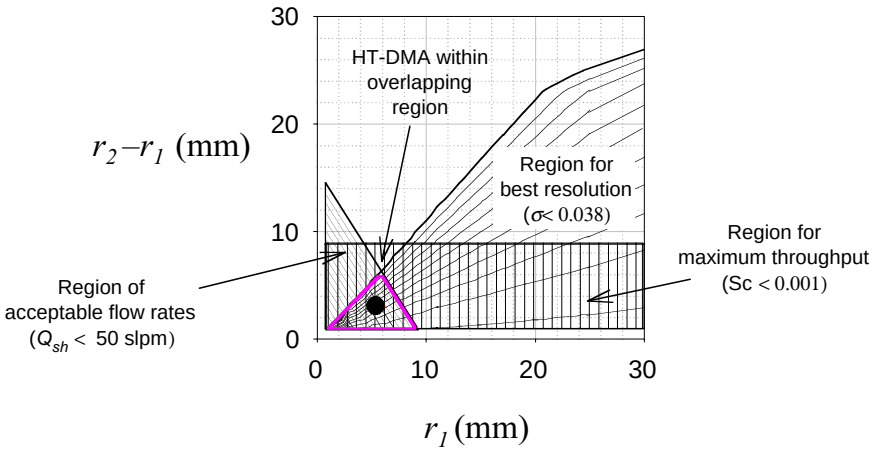

Fig. 5: Regions in the r_2 - r_1 vs. r_1 space where, according to Figs. 3 and 4 the space charge number Sc and the broadening parameter $\tilde{\sigma}$ are minimized for $L=L_{\min}$, D_p = 1 nm, Re = 2200, β = 0.01. Also shown is the region where flow rates are below 50 standard liters per minute. The geometrical parameters of our instrument were chosen within the overlapping region shown in the figure.

Incorporation of size classification into a materials deposition process

We have incorporated the size classification approach described above into a streamlined deposition process capable of creating homogeneous samples containing nanoparticles of uniform size. This process is depicted in Fig. 6. Gas-suspended nanoparticles generated by the ablation of a solid target go through an ionization zone where they acquire an equilibrium charge distribution. The charged nanoparticles are then sorted according to size based on their different migration velocities in an electric field across a particle-free laminar gas stream. Nanoparticles are extracted from the classification region within a desired window of sizes and deposited electrophoretically on a substrate placed perpendicularly to the gas flow.

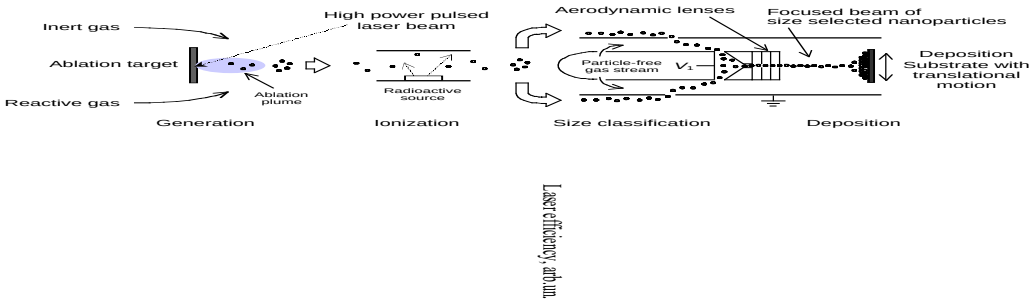

Fig. 6: Schematic showing the incorporation of the size classification approach into a laser ablation source of nanoparticles allowing the deposition of size-selected nanoparticles.

A schematic of the experimental setup implementing this deposition scheme may be seen in Fig. 7. In this case, an aerosol of silver (Ag) nanoparticles was obtained by the ablation of a Ag target in inert atmosphere by the focused beam of a pulsed Nd:YAG laser. The aerosol was then run through a small chamber containing a ^{241}Am radioactive source that created an equilibrium ion distribution in the carrier gas. This

allowed the charging of the nanoparticle aerosol. Charged nanoparticles where then introduced into the size classifier (DMA) and deposited on a silicon [110] surface. A sample obtained using this system is shown in Fig. 8, which displays Atomic Force Microscopy (AFM) scans. For this experiment nanoparticles were size selected at (8.0 ± 0.6) nm. Figure 8(a) illustrates the remarkable uniformity of the nanoparticle ensembles, which extends to regions several millimeters across while Fig. 8(b) shows a small area scan. The deposition of size-selected Ag nanoparticles establishes a benchmark performance for our system and we are currently employing this strategy for other materials with potential for aerospace applications.

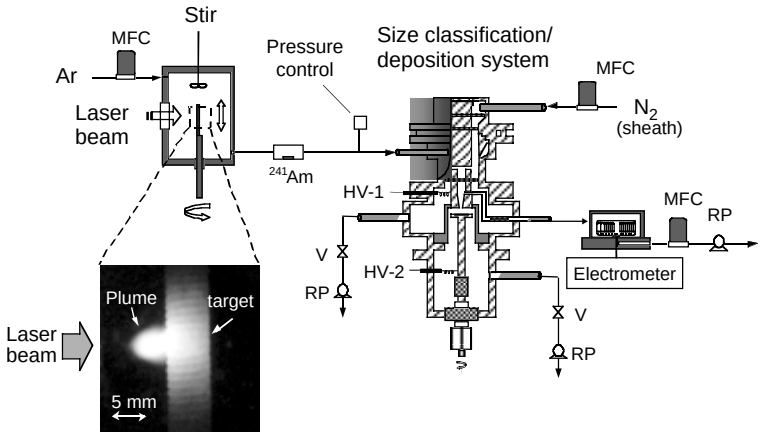

Fig. 7: Laser ablation setup used in combination with the size classifier to obtain nanostructured thin films.

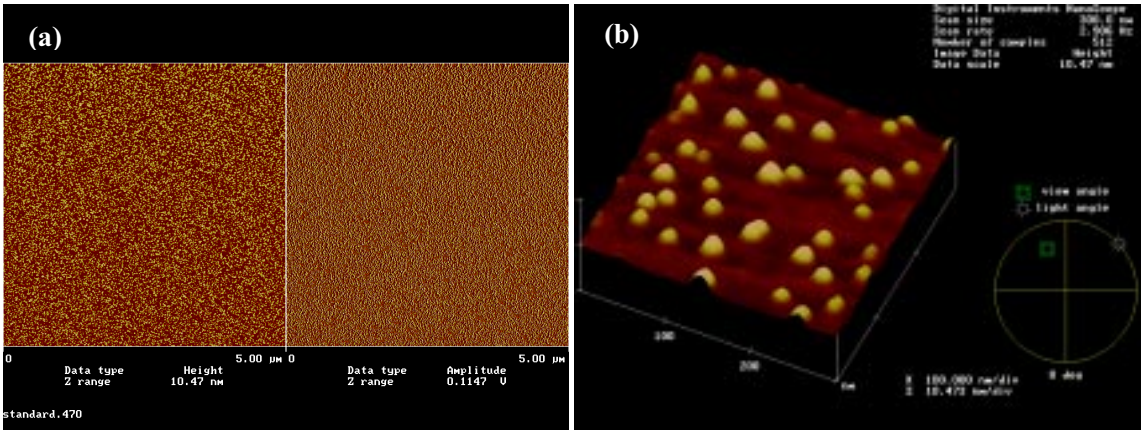

Fig. 8: Atomic Force Microscopy scans of size-selected Ag nanoparticles (8.0 ± 0.6 nm) deposited on a [110] silicon surface. (a) 5-micron scan (height and amplitude signals) and (b) 300-micron scan (3D view).

Acknowledgements

This research was supported in part by grants from the National Science Foundation (NSF) (MRI/DMR#0116098) and the National Aeronautics and Space Administration (Alabama NASA EPSCoR Core Infrastructure Development Program). Nicholas C. Cunningham acknowledges support from the NSF-funded Research Experiences for Undergraduates program at The University of Alabama at Birmingham (NSF-DMR# 0243640)

References

1. Alivisatos, A. P., *Science* **289**, 736 (2000).
2. Mirkin, C. A., Letsinger, R. L., Mucic, R. C., and Storhoff, J. J., *Nature* 382, 607 (1996).
3. Boeckl, M S; Baas, T; Fujita, A, *Biopolymers* **47**, 185 (1998).
4. Ueda, M.; Kreuter, J.**,** *Journal of microencapsulation* **14**, 593 (1997).
5. Li, M., Schnablengger, H., and Mann, S., *Nature* **402**, 393 (1999).
6. Camata, R. P., Atwater, H.A., Vahala, K. J., and Flagan, R. C., *Applied Physics Letters* **68**, 3162 (1996).
7. Dinh L. N., Chase, L. L., Balooch, M., Siekhaus, W. J., and Wooten, F. *Physical Review B* **54**, 5029 (1996).
8. Camata, R.P., Hirasawa, M., Okuyama, K., Takeuchi, K., *Journal of Aerosol Science* **31**, 391 (2000).
9. Knutson, E.O. and Whitby, K.T., *Journal of Aerosol Science* **6**, 453 (1975).
10. Flagan, R. C., Aerosol Science and Technology **28**, 301 (1998).
11. Allen, M. D. and Raabe, O. G., Journal of Aerosol Science 13, 537 (1982).
12. Deppert, K., Magnusson, M. H., Samuelson, L., Malm, J.-O., *Journal of Aerosol Science* **5**/**6**, 737 (1998)
13. Magnusson, M. H., Deppert, K., Malm, J.-O., Svensson, C. *, Journal of Aerosol Science* **28**, S471 (1997).
14. Kruis F.E., Fissan H., Peled A., *Journal of Aerosol Science* **29**, 511 (1998).
15. Seto T, Kawakami Y, Suzuki N., *J. Nanoparticle Research* **3**, 185 (2001).
16. Seto T, Kawakami Y, Suzuki N., *Nano Letters* **1**, 315 (2001).
17. R. P. Camata, H. A. Atwater, and R. C. Flagan, *Journal of Aerosol Science* **32**, 583 (2001).
18. Kousaka, Y., Okuyama, K., Adachi, M. and Mimura, T. *J. Chem. Eng. Japan* **19**, 401-407. (1986).
19. Stolzenburg, M.R., *An Ultrafine Aerosol Size Distribution Measuring System*, Ph.D. Thesis, University of Minnesota. (1988).
20. Zhang, S.-H and Flagan, R.C., *Journal of Aerosol Science* **27**, 1179 (1996).
21. Flagan, R.C., *Aerosol Science and Technology* **30**, 556 (1999).
22. De Juan, L., Fernandez de la Mora, J., *Journal of Aerosol Science.* **29**, 617 (1998).